Acta Pharmaceutica Sinica B 2024;14(6):2773–2785

Chinese Pharmaceutical Association
Institute of Materia Medica, Chinese Academy of Medical Sciences

Acta Pharmaceutica Sinica B

www.elsevier.com/locate/apsb
www.sciencedirect.com

ORIGINAL ARTICLE

Genome mining of sulfonated lanthipeptides reveals unique cyclic peptide sulfotransferases

Meng Wang[†], Wen-Wei Li[†], Zhe Cao, Jianong Sun, Jiang Xiong, Si-Qin Tao, Tinghong Lv, Kun Gao, Shangwen Luo[*], Shi-Hui Dong[*]

State Key Laboratory of Applied Organic Chemistry, College of Chemistry and Chemical Engineering, Lanzhou University, Lanzhou 730000, China

Received 31 October 2023; received in revised form 31 January 2024; accepted 7 February 2024

KEY WORDS

Lanthipeptides;
Sulfotransferases;
Sulfonation;
Biosynthesis;
Genome mining

Abstract Although sulfonation plays crucial roles in various biological processes and is frequently utilized in medicinal chemistry to improve water solubility and chemical diversity of drug leads, it is rare and underexplored in ribosomally synthesized and post-translationally modified peptides (RiPPs). Biosynthesis of RiPPs typically entails modification of hydrophilic residues, which substantially increases their chemical stability and bioactivity, albeit at the expense of reducing water solubility. To explore sulfonated RiPPs that may have improved solubility, we conducted co-occurrence analysis of RiPP class-defining enzymes and sulfotransferase (ST), and discovered two distinctive biosynthetic gene clusters (BGCs) encoding both lanthipeptide synthetase (LanM) and ST. Upon expressing these BGCs, we characterized the structures of novel sulfonated lanthipeptides and determined the catalytic details of LanM and ST. We demonstrate that SslST-catalyzed sulfonation is leader-independent but relies on the presence of A ring formed by LanM. Both LanM and ST are promiscuous towards residues in the A ring, but ST displays strict regioselectivity toward Tyr5. The recognition of cyclic peptide by ST was further discussed. Bioactivity evaluation underscores the significance of the ST-catalyzed sulfonation. This study sets up the starting point to engineering the novel lanthipeptide STs as biocatalysts for hydrophobic lanthipeptides improvement.

*Corresponding authors.
E-mail addresses: luosw@lzu.edu.cn (Shangwen Luo), dongsh@lzu.edu.cn (Shi-Hui Dong).
[†]These authors made equal contributions to this work.

Peer review under the responsibility of Chinese Pharmaceutical Association and Institute of Materia Medica, Chinese Academy of Medical Sciences.

https://doi.org/10.1016/j.apsb.2024.02.016

1. Introduction

Over the course of a century of development, peptide therapeutics have emerged as promising drug candidates, occupying a distinctive pharmaceutical niche between small-molecule drugs and biologics[1], as evidenced through numerous examples in clinical applications. Particularly appealing targets for pharmaceutical research include cyclic peptides and those containing disulfide bonds[2]. Lanthipeptides, a type of macrocyclic peptide, are characterized by post-translational modifications (PTM) involving lanthionine (Lan) and methyllanthionine (MeLan) cross-links (Scheme 1A)[3]. They represent the most abundant family of ribosomally synthesized and post-translationally modified peptides (RiPPs) to date. Lanthipeptides exhibit a diverse array of bioactivities, including anti-bacterial, anti-viral, and anti-fungal activities, among others[4]. A notable example undergoing clinical evaluation is microbisporicin, which has demonstrated exceptional antimicrobial activity against various major Gram-positive pathogens[5]. The formation of these macrocyclic PTMs is usually leader-dependent[3]. Furthermore, a range of structurally diverse secondary tailoring PTMs have been identified and characterized[3,4,6]. Notably, most of these PTMs consist of decoration of hydrophilic residues[3,4,6], which lead to increased hydrophobicity, improved chemical stability and enhanced bioactivity. However, these PTMs also result in decreased solubility[3], which poses a challenge for the clinical development of lanthipeptides[7-9].

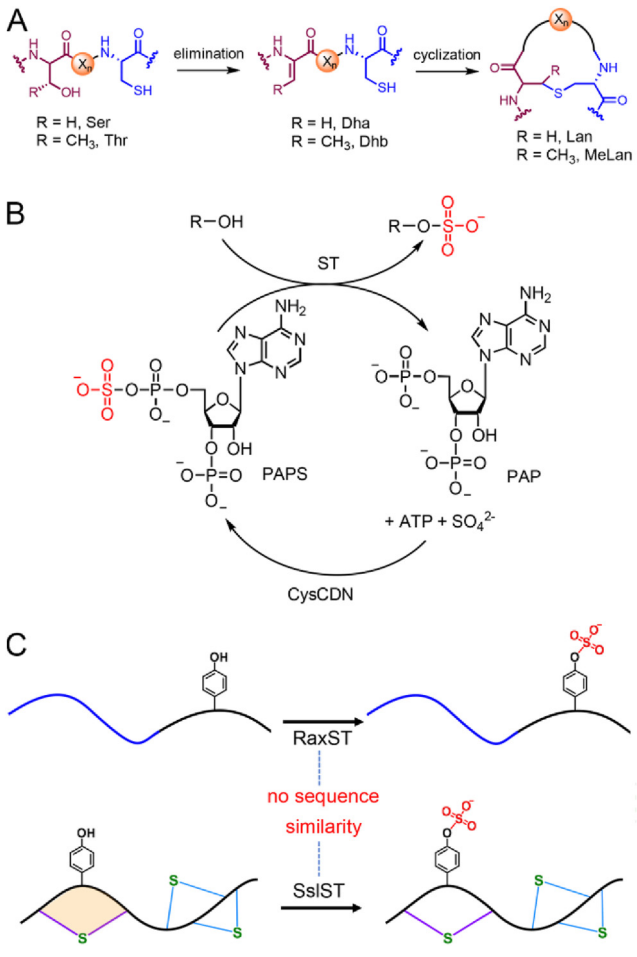

Scheme 1 (A) Schematic depiction of Lan and MeLan formation. (B) General ST-catalyzed sulfonation with PAPS as the sulfuryl group donor. CysCDN are PAPS biosynthetic enzymes. (C) Schematic diagrams of the RaxST- and SslST-catalyzed sulfonation. RaxST modifies the linear peptide before removal of the leader, whereas SslST is leader-independent and sulfonates cyclic peptide. Blue curves represent leader peptide.

Sulfotransferases (STs) catalyze the sulfonation or sulfurylation of biological molecules in living organisms and fulfill several essential roles in physiological processes, including detoxification, hormone regulation, drug metabolism, and pathogenicity[10]. STs transfer a sulfuryl group (SO_3) from an activated donor molecule, usually 3′-phosphoadenosine-5′-phosphosulfonate (PAPS), to a wide range of acceptor substrates with hydroxy or amine groups as nucleophiles (Scheme 1B). These substrates include both large biomolecules such as carbohydrates and proteins, and endogenous and exogenous small molecules such as steroids, bioamines, phenols, drugs, and various xenobiotic agents[10,11].

However, sulfonation is relatively rare and underexplored in secondary metabolism, especially in peptidyl natural products. Only a few members from the superfamily of RiPPs have been discovered to have sulfuryl decoration as a PTM (Supporting Information Fig. S1), such as the scarce cases in sulfonatyrotides[12], methanobactins[13,14], and conopeptides[15]. Sulfonatyrotide RaxX was isolated from the Gram-negative pathogen *Xanthomonas oryzae* pv. Oryzae (Xoo) and was found to be a robust activator of the eukaryotic host immune receptor[6,12,16-17]. The class-defining Tyr sulfonation in RaxX is catalyzed by RaxST, which works on a Tyr residue embedded in a linear peptide before removal of the leader (Scheme 1C)[12]. Methanobactins are copper-chelating RiPPs produced by methane-oxidizing bacteria *Methylocystis* spp. A small set of methanobactins are post-translationally modified with Thr sulfonation to increase their affinity to copper. However, the putative STs encoded in the biosynthetic gene clusters (BGCs) of methanobactins are yet to be characterized. In addition, the biosynthetic path of sulfotyrosines of conopeptides produced by cone snails remains unknown[4,6,18]. Collectively, peptidyl STs have rarely been characterized, not to mention the mechanistic details of their peptide recognition[6].

Sulfonation also stands out as a prevalent strategy in medicinal chemistry, employed to derivatize drug-like molecules with the aim of enhancing their water solubility and chemical diversity[19,20]. A noteworthy illustration of the efficacy of this approach is observed in minoxidil, an anti-hypertensive and hair growth-stimulating drug, where the sulfonated metabolite is attributed to its biological activity[21]. Intriguingly, despite the widespread application of sulfonation in various drug development contexts, this strategy has not yet been explored in lanthipeptides. Thus, we sought to explore novel sulfonated RiPPs and characterize their corresponding STs. To this end, we identified two potential sulfonated lanthipeptide BGCs by genome mining and co-occurrence analysis. Through *in vivo* reconstitution studies and *in vitro* enzymatic transformations, we found that the lanthipeptide STs preferably recognize thioether and disulfide-containing cyclic peptides instead of their linear counterparts as the substrate. We also demonstrated that these STs have a broad tolerance of amino acid variations adjacent to the target Tyr. Additionally, these STs catalyze sulfonation in a leader-independent manner. These properties can considerably facilitate the application of STs in combinatorial biosynthesis for the structure diversity expansion of RiPPs. Moreover, the corresponding sulfonated lanthipeptides were structurally characterized

and exhibited improved anti-inflammatory activities compared to those not sulfonated. These data highlight the significance of ST-catalyzed sulfonation in medicinal chemistry. Collectively, our work not only expands the structural diversity of the RiPP superfamily but also adds a new type of biocatalyst to the enzyme toolbox for the derivatization of various cyclic peptides.

2. Results and discussion

2.1. *Co-occurrence analysis identifies putative sulfonated lanthipeptide BGCs*

Our initial genome mining efforts using either the RaxST[12] or the putative methanobactin ST[13,14] as the query sequence did not yield any novel RiPP BGCs with STs, as all cognate BGCs were closely related (Supporting Information Fig. S2). Therefore, we conducted a bioinformatic analysis of various class-defining biosynthetic enzymes, such as lanthipeptide synthetases (LanB, LanM, LanKC, LanL, and LanY)[6], aiming to identify their potential co-occurrence with putative STs. Notably, only the analysis of the class II lanthipeptide synthetase LanM yielded positive results. A sequence similarity network (SSN)[22,23] was constructed for LanMs using a 40% sequence identity criterion to separate clusters (Supporting Information Fig. S3). This SSN was then utilized to generate a genome neighborhood network (GNN) in order to query neighboring genes for each LanM sequence[22,23].

As a result of the GNN analysis (Supporting Information Fig. S4), two unprecedented BGCs were identified in *Streptomyces cinnamoneus* DSM 41675 (*ssl*) and *Streptomyces* sp. CB02923 (*ssc*). Each BGC encodes a putative LanM, a ST, a group of PAPS biosynthetic enzymes (CysCDN), and transporters (Fig. 1A and Supporting Information Table S1). Neither of the two BGCs has peptidase gene, indicating that leader removal may be achieved by a peptidase located outside the BGC, which is commonly observed in lanthipeptide biosynthesis[24-26]. The unusual co-occurrence of LanM, ST, and CysCDN genes led us to hypothesize that these BGCs encode the production of unprecedented sulfonated lanthipeptides. A sequence alignment of the two putative precursor peptides, SslA and SscA, also indicated that they are likely to be the substrates for LanMs and STs. SslA and SscA share 80.0% sequence identity and show high sequence conservation from Phe17 to Cys13, including two Ser, three Thr, three Cys residues (Fig. 1B), which can presumably be modified by their cognate LanMs (Scheme 1A). In addition, the notable Tyr5 residue can potentially be a sulfonation site[3].

2.2. *Reconstitution of ssl BGC produces sulfonated lanthipeptides*

To characterize the products of these novel BGCs, we first cultured DSM 41675 strain in a panel of media, and analyzed the extracts by liquid-chromatography high-resolution mass spectrometry (LC−HRMS). Two mass peaks, exhibiting identical masses, were noted, indicative of the presence of two constitutional isomers. This observation aligns with the outcomes of following co-expression experiments. The molecular ion peaks correspond to peptides derived from Ile1 to Arg16 of SslA with 5-fold dehydration (Supporting Information Fig. S5), providing clues for the boundary between the leader and the core peptides. Furthermore, the bioinformatic analysis, conducted through the

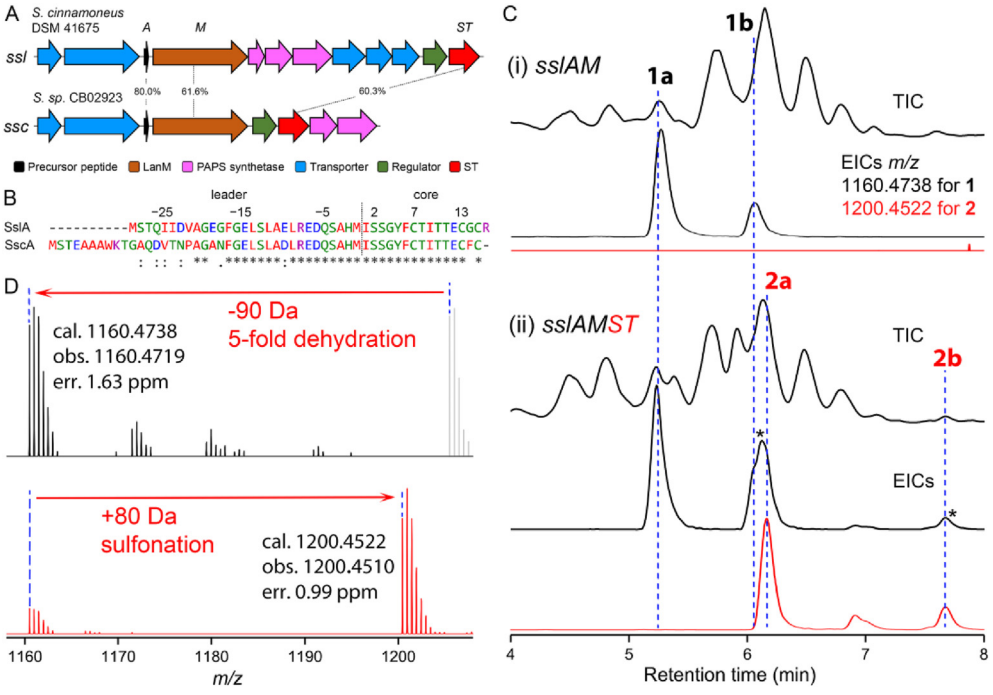

Figure 1 Reconstitution of the sulfonated lanthipeptide BGC. (A) BGCs of *Streptomyces*-derived sulfonated lanthipeptides, *ssl* and *ssc*. (B) Sequence alignment of SslA and SscA with the numbering and conservation of residues labeled on top and bottom, respectively. The grey line indicates the boundary between the leader and the core peptides. (C) The extracted ion chromatograms (EICs, less than 5 ppm deviation) of indicated co-expression. (i) co-expression of *sslA* and *sslM*; (ii) co-expression of *sslA*, *sslM*, and *sslST*. TIC, total ion chromatogram. *Denotes the peaks of sulfonated products that undergo desulfonation during ionization in LC−HRMS analysis. (D) Comparison of HRMS spectra of **1** (black) with the theoretical unmodified $SslA^{GluC}$ (grey) and **2** (red), respectively.

antiSMASH online server[27,28], predicted the leader-core boundary as our hypothesis. This convergence of results substantiates our proposed model with Ile1 as the start of the core peptide.

Because of the low yield of the native producing strain, we determined to clone and express the biosynthetic genes in *Escherichia coli* using codon optimized sequences. The precursor peptides were fused with His_6-maltose-binding protein (His_6-MBP) at the N-terminus. The M and ST proteins were tagged with His_6 (Supporting Information Table S2). His_6-MBP-SslA, His_6-SslM, and His_6-SslST were successfully purified from the soluble fractions (Supporting Information Fig. S6), whereas His_6-SscM and His_6-SscST were only found in the inclusion bodies. Therefore, the *ssl* BGC was prioritized for reconstitution.

A co-expression system using a pair of compatible vectors, pRSF-Duet and pCDF-Duet, was established to allow simultaneous expression of MBP-SslA, SslM, and SslST (Supporting Information Table S3). First, the co-expression of pRSF-MBP-SslA/SslM was attempted. The modified MBP-SslA was isolated by Ni-affinity chromatography and was subsequently treated with tobacco etch virus (TEV) protease for LC−HRMS analysis. MS data indicated the presence of two products with molecular ion peaks corresponding to 5-fold dehydration, namely $SslA^{M}{}_{Major}$ and $SslA^{M}{}_{Minor}$ (Supporting Information Figs. S7 and S8). Further digestion using the commercial protease GluC revealed the same dehydration patterns, and the two constitutional isomers were named as **1a** (major product, $SslA^{M/GluC}{}_{Major}$) and **1b** (minor product, $SslA^{M/GluC}{}_{Minor}$) (Supporting Information Fig. 1C−i, and D, top panel). Production of constitutional isomers were also observed in previous lanthipeptide studies[29,30]. The presence of five dehydrations indicated that all the Ser and Thr residues in the core peptide underwent dehydration (Fig. 1B and Scheme 1A). Incubation with thiol-reactive alkylating reagent *N*-ethylmaleimide (NEM) did not produce any alkylated adduct, indicating that all three Cys were involved in the formation of Lan/MeLan. This finding was consistent with the results from β-mercaptoethanol (βME) assays, which resulted in the formation of up to 2-fold βME adduct and established the existence of two dehydro-residues and three Lan/MeLan (Supporting Information Fig. S9). Next, we incorporated pCDF-SslST into the co-expression strain of pRSF-MBP-SslA/SslM to investigate the function of SslST. Following similar purification and treatment procedures, we observed two new peaks with molecular ion corresponding to sulfonated **1**, which were designated as **2a** ($SslA^{M/ST/GluC}{}_{Major}$) and **2b** ($SslA^{M/ST/GluC}{}_{Minor}$) (Fig. 1C−ii, and D, bottom panel). These findings confirm that the *ssl* BGC is capable of producing sulfonated lanthipeptide. Given that SslA and SscA share extremely similar core sequences with same numbers of Ser, Thr, Cys residues (Fig. 1B), we used pCDF-SscST to co-express with pRSF-MBP-SslA/SslM, which resulted in the production of **2a** and **2b** as well (Supporting Information Fig. S10). As all Ser, Thr, Cys residues are modified, we proposed that the sulfonation occurred at the hydroxy group of the Tyr5 side chain.

2.3. *Structural characterization of sulfonated lanthipeptides*

The HRMS/MS analysis of **1a** suggested the formation of Dha2 and one Lan between Cys7 and Dha3 (A ring), as well as two indistinguishable MeLan involving Cys13, Cys15, Dhb8, and Dhb10 or Dhb11 (Fig. 2A and Supporting Information Fig. S11). The tandem mass data of **1b** supported the assignment of A ring between Cys7 and Dha2 (Supporting Information Fig. S12). The difference between **1a** and **1b** was not due to the configuration of the Lan or MeLans, which was confirmed later. However, the HRMS/MS spectrum of sulfonated lanthipeptide **2a** resembled that of **1a** and did not provide any decisive fragmentation ions for the localization of the SO_3 group (Supporting Information Fig. S13), because of the lability of the SO_3 group during ionization[17]. To confirm our hypothesis that Tyr5 was sulfonated in **2**, a Y5F variant of SslA was constructed. Co-expression of MBP-SslA-Y5F with both SslM and SslST yielded products with 5-fold dehydration that were analogous to **1a** and **1b** (Supporting Information Fig. S14), whereas no sulfonated peptide was able to be detected. These data supported the proposed sulfonation site at the hydroxy group of Tyr5.

To further characterize the structures of the new sulfonated lanthipeptides by NMR, we removed all the leader peptide prior to NMR data acquisition to simplfy the spectra. To bypass the inaccessibility of the cognate peptidase, we constructed H-2R and M-1R variants of SslA to introduce Arg-1 or Arg-2 residue at the end of the leader peptide to be recognized by the commercial trypsin protease. Co-expression of MBP-SslA-H-2R with SslM and SslST produced only a small amount of protein. However, the yield of MBP-SslA-M-1R co-expression was comparable to that of wild type MBP-SslA, although only 4-fold dehydration was detected, which might result from the effect of the SslA M-1R mutation. The co-expression products after trypsin digestion (**3** and **4**) were purified by HPLC and subjected to tandem mass analysis and βME assays (Supporting Information Fig. S15), which supported the assignment that they were analogous to **1b** containing all three Lan/MeLan rings and an unmodified Ser3 (Fig. 2B). The ^{1}H NMR spectra of **3** and **4** showed substantial differences at the downfield region (Fig. 2C and Supporting Information Fig. S16). Compound **3** displayed two doublet signals at 6.61 ppm (H_2-6,8) and 6.89 ppm (H_2-5,9) for the side chain phenyl group and one singlet peak at 9.26 ppm for the hydroxy proton of Tyr5, whereas **4** only showed one broad signal for the four protons of phenyl group of Tyr5 at 7.01 ppm (H_2-5,6,8,9) and lacked the peak for the hydroxy group, supporting the hydroxy group of Tyr5 as the sulfonation site. Finally, analysis of the ^{1}H−^{1}H TOCSY and ROESY and ^{1}H−^{13}C HMBC spectra of **3** and **4** was carried out to determine the Lan/MeLan rings as shown in Fig. 2D (Supporting Information Figs. S17−S27), including the Lan (A ring) between Dha2 and Cys7 and two MeLan rings between Dhb8 and Cys13 (B ring) and between Dhb10 and Cys15 (C ring). Analogously, the structures of those related compounds were assigned (Fig. 2A and B).

To determine the absolute configurations of all residues, expecially the Lan and MeLan, in the newly discovered lanthipeptides, compounds **1a**, **1b**, **2a**, **2b**, **3**, and **4** were hydrolyzed for advanced Marfey's analysis[31,32]. The hydrolysates were derivatized with Marfey's reagents, L-FDLA (Nα-(5-fluoro-2,4-dinitrophenyl)-L-leucinamide). LC−MS analysis of the products and the derivatives of standards (synthetic LL-Lan, DL-Lan, L-*allo*-L-MeLan, and D-*allo*-L-MeLan, and nisin A hydrolysates containing DL-Lan and DL-MeLan) revealed that all obtained lanthipeptides contained DL-Lan (Fig. 2E and Supporting Information Fig. S28) and DL-MeLan (Fig. 2F and Fig. S28), and that all other residues are proteinogenic L-residues (Supporting Information Fig. S29).

2.4. *Biosynthetic order of three Lan/MeLan rings and leader-dependency of SslM*

To gain more insight into the catalytic characteristics of SslM in the new sulfonated lanthipeptide, the dehydration/cyclization

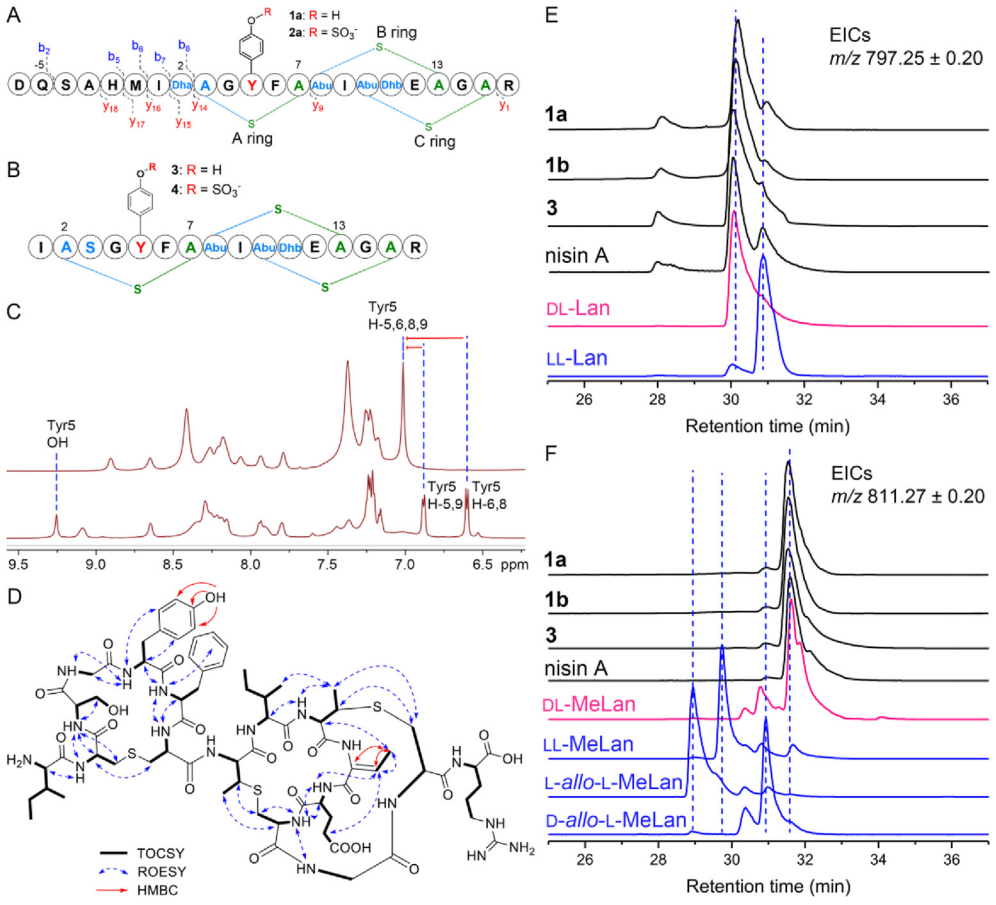

Figure 2 Structural characterization of the sulfonated lanthipeptides. (A) Schematic structures of **1a** and **2a** and the HRMS/MS analysis of **1a**. (B) Schematic structures of **3** and **4**. The HRMS/MS spectra of **1a**, **1b**, **2a**, and **3** are shown in Supporting Information Figs. S11−S13, and S15. (C) Comparison of ^{1}H NMR spectra (6.5−9.5 ppm) of **3** (bottom) and **4** (top). (D) 2D NMR analysis of **3**. Detailed NMR data of **3** and **4** are listed in Supporting Information Tables S4 and S5. Advanced Marfey's analysis of **1a**, **1b**, and **3** in comparison with nisin A hydrolysates and synthetic standards for determination of the absolute configuration of Lan (E) and MeLan (F). Compound hydrolysates and synthetic standards are derivatized with L-FDLA.

patterns and the leader sequence dependency of SslM were studied. A series of single-site Ala variants for each Ser, Thr, and Cys residues in SslA core region were constructed and co-expressed with SslM, which were then subjected to protease treatments, LC−HRMS analysis, and NEM assay. The SslM-modified products of SslA-C7A, SslA-C13A, and SslA-C15A variants diaplayed 5-fold dehydration and were not added with any NEM molecule, indicating that mutation of any one Cys had no effect on the formation of the other two rings. These results were further supported by HRMS/MS analysis of each product (Supporting Information Figs. S30−S32).

Products from the variants SslA-S2A and SslA-S3A showed mass peaks consistent with 4-fold dehydration. Tandem mass spectra and NEM assays supported that both products featured with three rings that were analogous to **1a** and **1b**, respectively (Supporting Information Figs. S33 and S34). Co-expression using the variant SslA-T10A produced 4-fold dehydrated product, which was added with one NEM. Tandem mass data of this product indicated a comparable structure with that of SslA-C15A (Supporting Information Fig. S35). The SslA-T8A and SslA-T11A variants only yielded a minimum amount of MBP-fused peptide and hence was not further investigated. These mutational studies agreed with the elucidated lanthipeptide structures, and also demonstrated the biosynthetic features of SslM-catalyzed Lan/MeLan formation, including (1) the dehydration reactions are not impacted by the mutation of any of the Ser, Thr, or Cys residues, and (2) the formation of three rings is independent to each other.

The leader-guided biosynthetic strategy is a unique feature of RiPP biosynthesis, in which PTM enzymes interact with leaders but catalyze PTMs on their cognate cores. To assess the essentiality of different leader regions in the biosynthesis of the new sulfonated lanthipeptide, we co-expressed various SslA variants with both SslM and SslST. We analyzed the resulting product profiles using LC−HRMS (Supporting Information Figs. S36−S42) and summarized the findings in Fig. 3A and B. The yields of products for each variant were compared to those obtained from wild-type SslA co-expression.

As illustrated in the sequence alignment (Fig. 1B), the N-terminal region of the leaders of SslA and SscA is less conserved, suggesting that it may not be critical for binding. To confirm this, we tested three truncation variants of SslA, in which the first 4, 9, and 14 residues were removed, respectively. These variants, named as △4SslA, △9SslA, and △14SslA (Fig. 3A), underwent comparable dehydration and sulfonation to wild-type SslA, with even higher yields. The △19SslA variant produced similar product

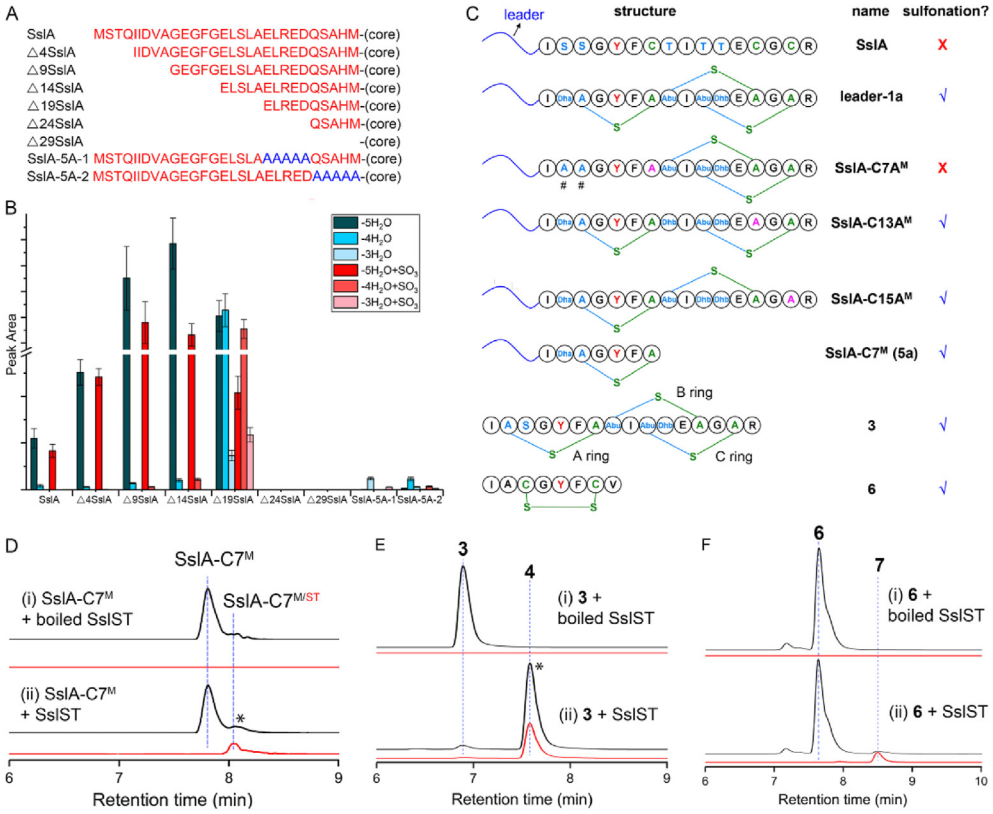

Figure 3 (A) SslA variants with leader mutations. (B) Summarization of product profiles from co-expressions of SslA leader variants with SslM and SslST. (C) Summarization of *in vitro* reactions of SslST. EICs of SslST *in vitro* reactions using (D) SslA-C7^{M}, (E) **3**, (F) and **6** as substrates. The EICs of substrates and products are presented in black and red, respectively. SslA-C7^{M}, SslA-C7$^{M/ST}$, **3**, **4**, **6**, and **7** are extracted using $[M + 3H]^{3+}$ ions of *m/z* 1376.6310 and 1403.2832, $[M + 2H]^{2+}$ ions of *m/z* 834.8520 and 874.8304, and $[M + H]^{+}$ ions of *m/z* 873.3634 and 953.3202, respectively, with less than 5 ppm deviation. *Denotes the peak of sulfonated product that undergoes desulfonation during ionization in LC-HRMS analysis. #Indicates the residues conjugated with glutathione.

profiles, except for larger amounts of 4-fold and 3-fold dehydration peptides and their sulfonated analogues. On the contrary, the use of the △24SslA and △29SslA variants completely abolished the production of dehydrated and sulfonated peptides (Fig. 3B), indicating that the C-terminal 10 residues of the leader are essential for SslM or SslST recognition. We then performed alanine scanning of these 10 residues using two variants, SslA-5A-1 and SslA-5A-2, replacing five residues with Ala between −10 and −6 and between −5 and −1, respectively (Fig. 3A). Co-expression of these two variants with SslM and SslST only yielded minimal amounts of dehydrated and sulfonated peptides (Fig. 3B), further validating the necessity of the C-terminal 10 residues of the leader during SslM or SslST catalysis.

2.5. In vitro *characterization reveals that lanthipeptide STs catalyze sulfonation on thioether cyclic peptides in a leader-independent manner*

The production of the sulfonated lanthipeptides through heterologous expression raised questions regarding the timing of Lan/MeLan formation and sulfonation. First, we performed *in vitro* reactions by incubating purified MBP-SslA with SslST, TEV, and CysCDN from *E. coli* (Scheme 1B and Fig. 1A), and detected only the intact SslA^{trypsin} without sulfonation by LC−HRMS (Supporting Information Fig. S43). As has been shown that SslM can directly modify SslA for Lan/MeLan formation, whereas SslST was not able to sulfonate SslA, we hypothesized that SslST catalyzes sulfonation after Lan/MeLan formation. To test this hypothesis, we performed a similar reaction in which SslA was replaced by SslM-modified SslA (**leader-1**). Expectedly, sulfonated lanthipeptide (**leader-2**) was successfully detected (Fig. 3C and Supporting Information Fig. S44). These data confirmed that SslST recognizes the ring structure and functions after SslM. These features are distinct from the STs involved in the biosynthesis of sulfonated proteins[10] and sulfonatyrotide[6,12,16,17], which modify linear peptides instead of cyclic peptides.

As there are three Lan/MeLan rings catalyzed by SslM, we then investigated the importance of each ring in SslST catalysis. We have identified three SslM-modified SslA variants, *i.e.*, SslA-C7A^{M}, SslA-C13A^{M}, and SslA-C15A^{M}, which lacks A, B, and C rings, respectively. Incubation of these variants with SslST would reveal the significance of each ring in sulfonation. *In vitro* reactions of SslST with each of the variants followed by subsequent LC−HRMS analysis showed the production of sulfonated peptides for SslA-C13A^{M} and SslA-C15A^{M}, whereas no sulfonated product was observed for SslA-C7A^{M} (Fig. 3C and Fig. S44). Similar results were obtained from co-expression experiments of these SslA variants with both SslM and SslST (Supporting Information Figs. S45−S47). These observations showed that the A ring plays a crucial role in SslST catalysis.

To gain further understanding of the role of C-terminal residues in SslST catalysis, a variant of SslA was created by removing

all the residues after Cys7, called SslA-C7. This variant was co-expressed with SslM, resulting in the production of two-fold dehydration products, namely SslA-C7^{M}. After treatment with trypsin, two compounds were detected and identified as **5a** and **5b** using HRMS/MS analysis together with βME and NEM assays (Supporting Information Fig. S48). Incubation of SslA-C7^{M} with SslST produced the sulfonated product, SslA-C7$^{M/ST}$ (Fig. 3C and D), although the yield was lower compared to the reaction using full-length substrate. Co-expression of MBP-SslA-C7 with SslM and SslST resulted in a similar product profile (Supporting Information Fig. S49). These results suggested that the C-terminal residues of the core are not essential for SslST catalysis but can enhance the catalytic efficiency.

Next, we investigated the necessity of the leader peptide for sulfonation catalyzed by SslST. The *in vitro* reactions of SslST using **3** as substrate achieved over 95% turnover to its sulfonated product **4** (Fig. 3C and E). These results unambiguously demonstrate that the SslST-catalyzed sulfonation is leader-independent, and that the cooperation of LanM and LanST represents another example of combinatorial biosynthesis using both leader-dependent and independent PTM enzymes.

Finally, a peptide with the sequence IACGYFCV was synthesized to further assess the substrate scope of SslST. This linear peptide was not a substrate of SslST as shown by the *in vitro* reaction at same condition (Fig. S44). The linear peptide was then oxidized to cyclic peptide **6** with a disulfide bond between Cys3 and Cys7. Incubation of **6** with SslST succesfully resulted in the production of sulfolnated product **7** (Fig. 3C and F). The expansion of substrate scope to include disulfide ring-containing peptide further underscores the potential of SslST as a promising biocatalytic tool for the derivatization of cyclic peptides.

2.6. Substrate promiscuity and regioselectivity of SslM and SslST

Having successfully shown that SslST recognizes and sulfonates Tyr5 in the A ring, we investigated the substrate promiscuity of SslM and SslST by testing if Gly4 and Phe6 in the A ring could be substituted to generate chemical diversity. We mutated Gly4 and Phe6 to other amino acids of different physicochemical properties and co-expressed the resulting variants with both SslM and SslST. The products were digested with TEV and analyzed by LC–HRMS (Table 1 and Supporting Information Figs. S50–S67). The substitution of Gly4 with hydrophobic residues (G4V, G4F, and G4W) resulted in less sulfonation, whereas the dehydration was not affected. The G4K variant yielded increased amount of 5-fold dehydration product, but a smaller amount of sulfonated product with 4-fold dehydration. The SslA-G4H, G4S, G4N, and G4D variants resulted in comparable or even higher yields of sulfonated species. Substituting Phe6 with Lys reduced the activity of SslM, resulting in a major product with 4-fold dehydration. The F6D and F6V variants produced decreased yields of both dehydration and sulfonation products. By replacing Phe6 with Tyr, the SslA-F6Y variant with two Tyr residues was generated, which produced a lower amount of mono-sulfonated product and no di-sulfonated product. Co-expressing the SslA-Y5F-F6Y variant, which exchanged Tyr5 and Phe6, completely eliminated sulfonated product production. SslA variants with replacement of Phe6 by Ala, His, Ser, Asn, or Trp were well modified to produce significant amount of sulfonated peptides. Overall, most substitutions at both positions were well tolerated by both SslM and SslST, with varying yields, and SslST was demonstrated to have strict regioselectivity toward the position of Tyr in the A ring.

Table 1 Summary of substrate promiscuity of SslM and SslST. Relative activities of SslM and SslST were quantitively estimated by comparing the intensity of dehydration and additional sulfonation products. + stands for the successful detection of the specified products; −indicates no detectable peptides observed. The corresponding mass spectra are shown in Supporting Information Figs. S8 and S50–S67.

Variants	Activity of SslM			Activity of SslST		
	$-5H_2O$	$-4H_2O$	$-3H_2O$	$-5H_2O+SO_3$	$-4H_2O+SO_3$	$-3H_2O+SO_3$
SslA	+++	+	−	++	−	−
G4V	+++	−	−	+	−	−
G4F	+++	+	−	+	−	−
G4W	+++	+	−	+	−	−
G4K	++++	++	−	−	+	−
G4H	++++	+	−	++	−	−
G4S	++++	−	−	+++	+	−
G4N	+++	−	−	++	−	−
G4D	++++	+++	+	++	+	−
F6K	+	+++	−	+	++	+
F6V	+	+	−	+	−	−
F6D	++	+	+	+	−	−
F6Y	+++	+	−	+	−	−
Y5F/F6Y	++++	+	−	−	−	−
F6A	+++	−	−	++	+	−
F6H	+++	+	−	+++	+	−
F6S	++	+	−	+++	+	−
F6N	+++	+	−	++	+	−
F6W	++	−	−	++	−	−

2.7. *Insights into the molecular basis for the recognition of cyclic peptide by SslST*

As the biochemical characterization demonstrated the distinct substrate preference of SslST, the molecular basis for the recognition of cyclic thioether peptide without leader peptide by the lanthipeptide sulfotransferase was investigated. Neither SslST nor SscST exhibits detectable sequence similarity to the characterized RaxST, which sulfonates a linear peptide before removal of the leader[12], or to the putative methanobactin STs[13]. To investigate the prevalence of the newly discovered STs, an SSN was built for SslST and SscST. Surprisingly, they were found at the outlier of the largest cluster when 60% sequence identity threshold was applied (Supporting Information Fig. S68). The corresponding GNN revealed that SslST and SscST are the only two members of their class co-localized with LanM. To provide an overall understanding of the relationship between lanthipeptide sulfotransferases and the other isozymes, a phylogenetic tree was built for SslST, SscST, and other characterized STs involved in natural product biosynthesis, including RaxST[12], MbnS[13-14], TotS[33], SulN[34], CcSULT[20], StaL[35], CurM-St[36], Cpz8, Cpz4[37], as well as two human tyrosylprotein STs[38], TPST1 and TPST2. Not surprisingly, SslST and SscST were located in a distinct clade (Supporting Information Fig. S69), which is in complete agreement with their undetectable sequence similarity and disparate substrate selectivity.

To visualize the binding mode of SslST and **3** or **4**, we attempted crystallization of SslST in the absence or presence of PAP, Mg^{2+}, and **3** or **4**. Unfortunately, no diffractable crystal was able to be obtained. Instead, an AlphaFold model of SslST was established (UniProt identifier, AF-A0A2G1XES1-F1; Fig. 4A)[39,40]. Comparison of SslST with other enzymes in the protein data bank (PDB) *via* the Dali server[41] reveals that the closest structural relative to SslST is the TPST1 involved in post-translational tyrosine sulfonation of proteins in complex with PAP and gastrin peptide (PDB, 5wrj; Supporting Information Fig. S70). They shared conserved domains for PAPS binding, whereas the peptide binding domains (PBDs) were completely non-superimposable (Fig. 4A), reflecting their different substrate preference, cyclic peptide for SslST and linear peptide for TPST1.

The minimal substrate containing only the A ring of **3**, designated as **8** (Fig. 4B), was modeled into the PBD of SslST to provide an overall picture. The structure of **8** was embedded into the cavity that was formed by two helix bundles with one ranging from His187 to Ala241 and the other comprising Glu33 to Asp143 (Fig. 4C and Supporting Information Fig. S71). The sidechain phenol of Tyr5 pointed towards and was in closest proximity to the superimposed 5′-phosphate group of PAP for sulfonation to occur.

The conserved residues of SslST involved in PAPS interaction were individually mutated to Ala and the resultant variants were evaluated for the sulfonation activity *in vitro* using **3** as substrate (Fig. 3C). The R12A mutation completely abolished the activity of SslST, and SslST-T16A and S183A variants only retained minimal efficacies (Fig. 4D and E, and Supporting Information Fig. S72), supporting the reliability of the SslST model. Next, we investigated the significance of residues that surrounded the putative peptide binding cavity (Fig. 4E and F). In the dock model, side chains of SslST Glu33 and Phe190 pointed to the Tyr5 of **8**, and their involvement in substrate recognition was demonstrated by *in vitro* reactions of the four corresponding variants SslST-E33A, E33W, F190A, and F190W, which were shown to be inactive. Glu76 and Tyr153 of SslST packed on the side of the Tyr5 of **8**, and E76A and Y153W variants had no effect on the yield of **4**, whereas E76W variant was dead and Y153A variant showed reduced activity (Supporting Information Fig. S73). Gly189 and Ile193 resided at the left side of the cavity, and when they were mutated to Trp, the variants completely lost the sulfonation activity. On the other side of the pocket, Asn36 was identified and mutated to Trp, and the resulted N36W variant could not produce **4**. Similarly, mutation of Ala64 at the back of the cavity to Trp resulted in a dead variant (Supporting Information Fig. S74). We further mutated two residues at the edge of the cavity, Gly40 and

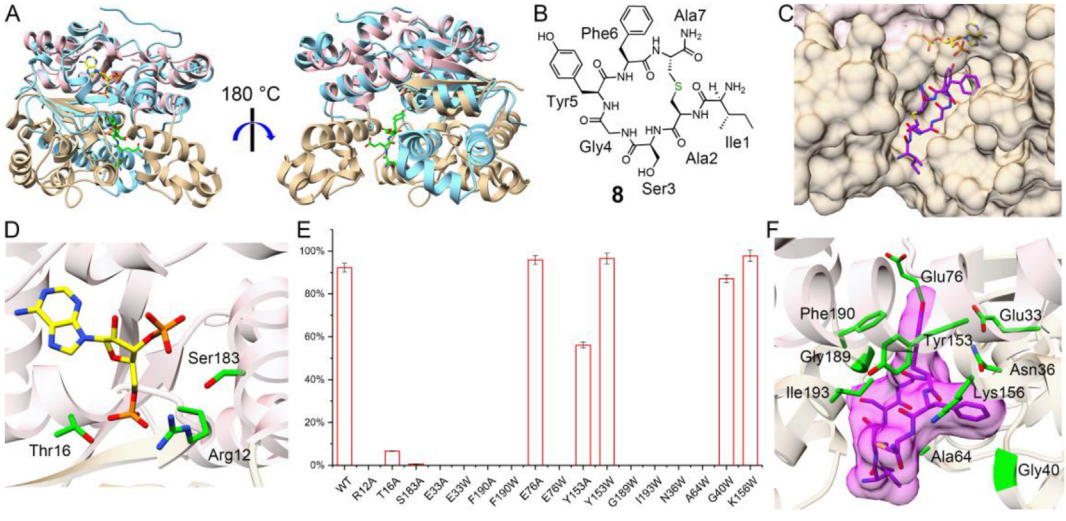

Figure 4 Characterization of the putative binding site of lanthipeptide in SslST. (A) Superimposition of the SslST model and complex structure of TPST1 with PAP and gastrin peptide. The PAPS binding doamin and PBD of SslST, TPST1, PAP, and gastrin peptide are showed in pink, tan, cyan, yellow, and green, respectively. (B) Chemical structure of **8**. (C) The dock model of **8** in PBD of SslST shown in surface model. (D) Representative key residues (green sticks) involved in PAP binding. The PAP structure was obtained from the superimposition with TPST1 complex structure. (E) *In vitro* transformation of **3** to **4** catalyzed by SslST and variants. The heights of the red bars represent the yields of **4**. (F) Identified key residues surrounding the putative cyclic peptide (purple sticks and surface) binding cavity.

Lys156 to Trp, and the resulted variants showed comparable activities with the wild type SslST (Fig. 3C and Supporting Information Fig. S75). Altogether, these results delineate a potential binding pocket in SslST for the lanthipeptide to be sulfonated.

2.8. *Bioactivity evaluation indicates the significance of the sulfonation*

Following characterization of the biosynthetic details, we evaluated the biological activity of purified lanthipeptides **3** and **4** to gain insights into the significance of sulfonation. Neither **3** nor **4** exhibited inhibition activity at 50 μmol/L against a panel of bacteria, or at 20 μmol/L against tumor cell lines HepG2 and LoVo. We also evaluated their anti-inflammatory activities by measuring their inhibitory effects on lipopolysaccharide-induced NO release in RAW264.7 macrophages. At a concentration of 40 μmol/L, **4** displayed an inhibition rate of about 51%, whereas **3** showed no activity with an obvious inhibition rate of about −2.3% (Supporting Information Fig. S76). Comparison of the inhibition rates and the chemical structures suggested that the sulfonate group enhanced the anti-inflammatory activity.

3. Conclusions

Due to the crucial role of macrocyclization of peptides and sulfonation in medicinal chemistry, we have identified the first BGCs of sulfonated lanthipeptide and characterized their encoded products, the biosynthetic order, the catalytic features, and the substrate tolerance of the PTM enzymes. Heterologous expression of the core biosynthetic genes confirmed our co-occurrence analysis that BGCs containing both LanM and ST genes would encode sulfonated lanthipeptides. Structure elucidation experiments revealed the positions of three Lan/MeLan rings (A, B, and C), and the sulfonation site at Tyr5 of the resulted lanthipeptides. The characteristics of SslM-catalyzed Lan/MeLan ring formation was explored through site-specific mutagenesis of key residues in the core peptide. Our *in vitro* enzymatic reactions unambiguously supported that SslST catalyzes sulfonation in a leader-independent and thioether or disulfide ring-dependent manner. Conversely, the activities of LanM rely on the C-terminal 10 residues of the leader. In addition, we found that both LanM and ST are promiscuous towards the substitution of residues in A ring, and that SslST sulfonation is highly regioselective toward Tyr5. Moreover, SslST is also able to sulfonate the analogous disulfide ring-containing peptide. Our bioactivity evaluation highlighted the positive effect of the sulfonate group. Considering these biosynthetic features and the bioactivity enhancement associated with the sulfonate group, our findings provide a foundational platform for the biocatalytic sulfonation of various cyclic peptides in drug development.

4. Experimental

4.1. *General materials and methods*

The genes and primers were synthesized by Xi'an Qingke Biotechnology Co., Ltd. and General Biosystems Co., Ltd., respectively. Restriction endonucleases, and Ready-to-Use Seamless Cloning Kits were purchased from Sangon Biotech (Shanghai) Co., Ltd. Phanta Max Super-Fidelity DNA Polymerase was purchased from Nanjing Vazyme Biotech Co., Ltd. *E. coli* DH5α and *E. coli* BL21 (DE3) were used for plasmid maintenance and protein overproduction, respectively. Chemical reagents were purchased from Sangon Biotech (Shanghai) Co., Ltd. The IACGYFCV peptide was purchased from Nanjing Yuanpeptide Biotech Co., Ltd. (Nanjing, China). DNA sequencing was performed by Xi'an Qingke Biotechnology Co., Ltd. pRSFDuet and pCDFDuet vectors were purchased from Sigma−Aldrich. pET N-terminal His6 TEV LIC and pET His6 MBP TEV LIC vectors were gifts from Scott Gradia (Addgene plasmid #29666 and #29656, respectively). All co-expression and *in vitro* enzymatic reactions were repeated at least three times. Cell Counting Kit-8 (CCK8) was purchased from Apexbio Technology LLC.

4.2. *Molecular biology techniques*

The DNA fragments of target genes were PCR-amplified using the *E. coli* BL21 (DE3) gDNA or codon-optimized and synthesized DNA as template by high fidelity Phanta Max Super-Fidelity DNA Polymerase. Amplification products were confirmed by 1.2% agarose gel electrophoresis, and purified using spin columns. The selected vectors were digested with selected restriction enzymes for 3 h at 37 °C using a water bath. The resulting DNA products and linearized vectors were assembled with Ready-to-Use Seamless Cloning Kit. *E. coli* DH5α cells were transformed with 5 μL of the assembled products by heat shock, and cells were plated on LB agar plates supplemented with appropriate antibiotics and grown for overnight at 37 °C. Several colonies were picked and used to inoculate separate 5 mL cultures of LB medium. The cultures were grown at 37 °C for 16 h before plasmids extraction. The sequences of the genes in the resulting plasmids were confirmed by DNA sequencing. The protein sequences and IDs were shown in Table S1. Primers used in this study were listed in Table S2. All plasmids used in this study were listed in Table S3.

4.3. *Bioinformatics*

The target sequence was used as seed for SSN construction using the "Sequence BLAST" option of the EFI-EST tools (UniProt Version: 2022_04)[23,42,43]. Then alignment scores corresponding to 35% sequence identity were used for final SSN generation. The 100% representative node network was opened and analyzed by Cytoscape[44], and 55%, 41%, 40%, and 60% sequence identity were applied to separate the clusters of SSN for RaxST, ST from *Methylocystis rosea* SV97, LanM, and SslST, respectively. Nodes were shown in different colors based on the size of each cluster. All ST sequences were inputted to Mega11 to construct the Maximum-likelihood tree[4].

4.4. *Cultivation of* S. cinnamoneus *DSM 41675*

The strain was purchased from the CGMCC (4.3578) strain collection, whereas *S.* sp. CB02923 was not available. The freeze-dried powder of the strain was inoculated into TSB media (5.95 g tryptone, 1.05 g peptone, 0.875 g glucose, 1.75 g NaCl, 0.875 g K_2HPO_4, 350 mL deionized water, pH 7.3), which was cultivated for approximately 3 days at 220 rpm and 30 °C. Then the obtained seed cultures were evenly used to inoculate four different freshly prepared media, including PTM (14 g dextrin, 14 g lactose, 1.75 g yeast extract, 0.7 g $CaCO_3$, 350 mL deionized water, pH 7.3), M15 (10.5 g glucose, 0.35 g peptone, 1.75 g beef extract, 1.75 g NaCl, 0.875 g $CaCO_3$, 350 μL trace elements, 350 mL deionized water, pH 7.3), MB (0.7 g

tryptone, 3.5 g glucose, 1.75 g soluble starch, 0.7 g yeast extract, 1.4 g NaCl, 0.175 g K_2HPO_4, 0.175 g $MgSO_4 \cdot 7H_2O$, 0.7 g $CaCO_3$, 350 mL deionized water, pH 7.3), and MD (3.5 g glucose, 1.75 g tryptone, 1.75 g yeast extract, 3.5 g glycerol, 1.05 g $CaCO_3$, 350 mL deionized water, pH 7.3). After 7 days of cultivation, the cultures were harvested by centrifugation, and the supernatants were extracted by *n*-butanol (*v*/*v*, 1:1). The resulted crude extracts were dried and re-dissolved in methanol of 15-fold less volume for LC−HRMS analysis.

4.5. Protein expression and purification

The plasmids with constructs of interest were transformed into *E. coli* BL21 (DE3) cells for protein expression. Cells were grown for 24 h on Luria-Bertani (LB) agar plates containing corresponding antibiotics at 37 °C. Single colonies were picked to inoculate 10 mL of LB containing corresponding antibiotics and grown at 37 °C for 16−18 h. This culture was used to inoculate 1 L of LB containing appropriate antibiotics and grown to an optical density at 600 nm (OD_{600}) of 0.6−0.8 and then placed on ice for 20 min. Isopropyl *β*-D-1-thiogalactopyranoside (IPTG) was then added to a final concentration of 0.5 mmol/L, followed by an induction period at 18 °C for 18 h. Notably, induction was proceeded at 30 °C for 18 h for the co-expression experiments, leading to higher titer of the modified peptides. Cells were harvested via centrifugation at 6000 × *g* for 20 min and resuspended in 30 mL suspension buffer [500 mmol/L NaCl, 20 mmol/L Tris pH 8.0, 10% glycerol (*v*/*v*)]. Cells were lysed by sonication (1 s on, 2 s off) at 50% amplitude in ice water. Insoluble cell material was removed by centrifugation at 12,000 × *g* for 30 min at 4 °C. The resultant supernatant was loaded onto a pre-equilibrated NiNTA-HisTalon μSphere column (Wuxi Tianyan Biotechnology Co., Ltd.). The column was washed with 40 mL wash buffer containing 1 mol/L NaCl, 20 mmol/L Tris pH 8.0, and 30 mmol/L imidazole. Then the column was eluted with 40 mL elution buffer containing 1 mol/L NaCl, 20 mmol/L Tris pH 8.0, and 250 mmol/L imidazole with 5 mL each fraction. The resultant fractions were examined visually by Coomassie-stained sodium dodecyl sulfonate polyacrylamide gel electrophoresis (SDS-PAGE) gel. A buffer exchange with protein storage buffer [20 mmol/L Tris, pH 8.0, 300 mmol/L NaCl, 10% glycerol (*v*/*v*)] was performed prior to concentration. The exchanged solution was concentrated using a 10 kDa molecular weight cut-off (MWCO) Amicon Ultra centrifugal filter. Protein concentrations were determined using 280 nm absorbance (theoretical extinction coefficients were calculated using the ExPASy ProtParam tool; http://web.expasy.org/protparam/). Purity was visually inspected by Coomassie-stained SDS-PAGE gel.

4.6. N-Ethylmaleimide (NEM) assays

A 100 μL aliquot of the reaction solution contained 200 μmol/L peptide, 10 mmol/L TCEP, 10 mmol/L NEM, and 50 mmol/L Tris-HCl (pH 7.5), which was incubated in 30 °C water bath for 1 h in dark. The reactions were further analyzed by LC−HRMS.

4.7. β-Mercaptoethanol (βME) assays

A 100 μL aliquot of the reaction solution contained 200 μmol/L peptide, 500 mmol/L NaCl, 1 mmol/L TCEP, 50 mmol/L βME, and 50 mmol/L Tris-HCl (pH 9.0), which was incubated in 30 °C water bath for 3 h in dark. The reactions were further analyzed by LC−HRMS.

4.8. In vitro enzymatic activity assays of SslST

The IACGYFCV peptide was stirred at room temperature for overnight with a concentration of 2 mmol/L. The resultant mixture was purified by HPLC and the disulfide-containing peptide was combined based on the HRMS data. A 200 μL aliquot of the reaction solution contained 200 μmol/L peptide, 5 mmol/L $MgSO_4$, 5 mmol/L ATP, 100 mmol/L K_2HPO_4, 50 mmol/L HEPES (PH 8.0), 0.5 U/mL inorganic pyrophosphatase, 10 U/mL pyruvate kinase, 75 mmol/L phosphoenolpyruvate, 10 μmol/L E. *coli* CysCDN, 10 μmol/L TEV (when MBP fused peptides were used), and 10 μmol/L SslST, which was incubated in 30 °C water bath for 12 h. The reactions were quenched by addition of equivalent volume of acetonitrile with 0.1% TFA, and the supernatant was obtained after centrifugation for lyophilization. The samples were dissolved in 200 μL of chromatography-grade methanol for analyzation by LC−HRMS.

4.9. Peptide expression and purification

The *cysCDN* genes were cloned into pCDFDuet-*sslST* and pACYCDuet vectors for co-expression with *sslAMST*. This co-expression strategy yielded sulfonated lanthipeptides with comparable yields to the system without additional cysCDN genes. MBP-SslA and variants co-expressed with SslM and/or SslST were purified following the similar protocol for protein expression and purification, except the removal of glycerol from the storage buffer. The obtained MBP-peptide solution was treated with TEV for 5 h at 37 °C water bath to cleave peptide from MBP, which was precipitated by addition of acetonitrile with 0.1% formic acid (1:1, *v*/*v*). Then, the supernatant was obtained by centrifugation and dried by lyophilization, and the resultant material was redissolved in enzymatic reaction buffer with GluC or trypsin for leader digestion. The protein was precipitated and the supernatant was harvested for further analysis by LC−HRMS or purification by HPLC. Compounds **3** and **4** were obtained from the co-expression of MBP-SslA-M-1R with SslM and SslST, and the product was treated with trypsin after TEV cleavage, which was purified by HPLC (Shimadzu, LC-20A) equipped with a C18 reversed phase column (Shimadzu, Shim-pack GIST C18, 5 μm, 100 Å, 4.6 mm × 250 mm) using a gradient from 40% methanol with 0.1% formic acid to 100% methanol with 0.1% formic acid over 25 min. Compounds **3** and **4** were eluted at 16.0 and 17.4 min with the yield of 9.0 and 7.8 mg from 24 L cultures, respectively.

4.10. HRMS data acquisition

LC−HRMS data was recorded on a ThermoFisher Scientific, Q Exactive mass spectrometer. Separation was performed on an AcclaimTM 120 C18 3 μm 120 Å (3 mm × 150 mm) column running at 0.3 mL/min. Mobile phases were solvent A (0.1% formic acid in water) and solvent B (0.1% formic acid in methanol). For detection of TEV-cleaved peptides, the following gradient was used unless specified otherwise: 50%−100% B over 10 min. When the peptides were further digested with GluC or trypsin, the gradient was adjusted to 40%−100% B over 10 min. For mass spectrometry, the instrument was set to run in positive mode with mass range 200−3000 *m*/*z* and the following parameter. Sheath gas flow rate: 35 mL/min; Aux gas flow rate: 10 mL/min; Sweep gas flow rate: 1 mL/min; Spray voltage: 4.00 kV; Capillary temperature: 320 °C; Aux gas heater temperature: 30 °C. For MS/MS, the

instrument was set to run Auto MS^2 mode and fragmented at 20−30 V collision energy.

4.11. NMR data acquisition of **3** and **4**

Compounds were dissolved in 150 μL of DMSO-d_6 and transferred into heavy wall NMR tubes. All NMR spectra were acquired using a Bruker AVANCE NEO 600 spectrometer. The ^{1}H, ^{1}H−^{1}H COSY, ^{1}H−^{1}H TOCSY, ^{1}H−^{13}C HSQC, ^{1}H−^{13}C HMBC, and ^{1}H−^{1}H NOESY spectra of **3** were acquired using 240, 26, 28, 180, 320, and 32 scans, and those of **4** were acquired using 240, 26, 28, 180, 280, and 32 scans.

4.12. Antibacterial activity of **3** and **4**

Antibacterial activity of **3** and **4** were evaluated using disc diffusion method following the published protocols[45]. A panel of bacterial strains were used, including *E. coli* K12, *E. coli* MG1655, *E. coli* ATCC 25922, *Acinetobacter baumannii* ATCC 19606, *Klebsiella pneumoniae* ATCC 13883, *Staphylococcus aureus* Newman, *S. aureus* ATCC 29213, *Staphylococcus cohnii* DKG4, *Staphylococcus simulans* AKA1, *Enterococcus faecalis* ATCC 29212, *Enterococcus gallinarum* 5F52C, *Bacillus subtilis*, *Bacillus thuringiensis*, *Micrococcus luteus*, *Pseudomonas aeruginosa*, *Clostridium perfringens* FSKP20, *Salmonella typhimurium* SH138, *Salmonella heidelberg* SH36, and *Proteus mirabilis* SG0508. The strains were cultured in LB overnight at 37 °C (220 rpm). Subsequently, 20 μL aliquots of the respective seed cultures were inoculated into 2 mL of fresh LB media, which were grown at 37 °C (220 rpm) until the OD reached 0.4. Next, 50 μL of the cultures were added to 100 mL of heated LB agar, which was cooled to approximately 50 °C, mixed, and poured into sterilized plates. Sterilized filter paper with a diameter of 5 mm was placed on the surface of the solid LB agar, and 10 μL of 50 μmol/L test compound solutions in water were added to the filter paper. The plates were then incubated at 37 °C for 18−24 h to observe the inhibition zones. Unfortunately, no inhibition zone was observed for both compounds.

4.13. Cytotoxic activity of **3** and **4**

They were assessed for cytotoxicity against HepG2, LoVo, and RAW264.7 macrophage cells by the CCK8 assay. 100 μL of different cells were plated in a 96-well flat bottom tissue culture plate at a density of 3×10^4 cells/mL (for HepG2 and LoVo) or 8×10^5 cells/mL (for RAW264.7) in medium containing 10% fetal bovine serum and allowed to adhere overnight at 37 °C in 5% CO_2. DMEM medium was used for HepG2 and RAW264.7, and RPMI-1640 medium was used for LoVo. The cells were treated by adding 100 μL of compound solution to reach the final concentration of 20 μmol/L. All compounds were dissolved in DMSO (0.1%), and DMSO (0.1%) was used as negative control. After 24 h, the cell viability assay (CCK8 assay) was carried out. 10 μL of CCK8 was added to each well, and cells were incubated for additional 1 h at 37 °C. Then optical density (OD) was measured at wavelength of 450 nm using a multimode microplate reader (BioTek Synergy Neo2).

4.14. Measurement of nitric oxide content

NO production was determined by the level of nitrite in the culture medium using the Griess assay[46]. Briefly, RAW264.7 macrophage cells were seeded in 96-well plates (8×10^5 cells/mL, 100 μL) for 12 h and pretreated with the test compounds for 2 h. LPS (10 μg/mL) was then added, and L-NMMA (Sigma) was used as the positive control. After 24 h, 80 μL of the supernatant from incubates was then added to 100 μL of an equal volume of mixed Griess reagent A and Griess reagent B (Beyotime Biotechnology, China) and cultured 10 min at 37 °C under dark conditions. The absorbance was measured at 540 nm by a multimode microplate reader (BioTek Synergy Neo2).

4.15. Synthesis of standard Lan and MeLan

Synthesis of LL-Lan, DL-Lan, L-*allo*-L-MeLan, and D-*allo*-L-MeLan was performed by a procedure similar to a previous report (Supporting Information Schemes S1−S3)[47]. Briefly, acetyl chloride (1.8 mL, 25.2 mmol, 3.0 equiv) was slowly added to MeOH (12 mL) at 0 °C. The solution was stirred for 15 min, followed by addition of L-serine, D-serine, L-threonine, D-threonine, L-*allo*-threonine, D-*allo*-threonine (1.0 g, 8.4 mmol, 1.0 equiv). After refluxing for 3 h, the solution was cooled to room temperature, and evaporated under reduced pressure to yield methyl esters.

Each of the methyl esters was resolved in water (5 mL), and the solution was then adjusted to pH 7.0 by saturated aqueous $NaHCO_3$, followed by addition of K_2CO_3 (1.1 g, 8.0 mmol, 1.0 equiv). After addition of the solution of Boc_2O (2.1 mL, 9.6 mmol, 1.2 equiv) in tetrahydrofuran (5 mL), the mixture was stirred for 16 h. THF was evaporated and the aqueous solution was extracted with ethyl acetate (3 × 10 mL). The organic fraction was washed with water and brine, dried over $MgSO_4$, filtered and evaporated under reduced pressure to yield L-Lan-**2**, D-Lan-**2**, L-MeLan-**2**, L-*allo*-MeLan-**2**, D-MeLan-**2**, and D-*allo*-MeLan-**2**.

$SOCl_2$ (1.4 mL, 18.8 mmol) was added to degassed CH_3CN (10 mL) in a dry round bottom flask under nitrogen. The solution was cooled to −42 °C. Boc-serine ester or boc-threonine ester (7.5 mmol) in degassed CH_3CN (10 mL) was added dropwise in 30 min. After the addition of pyridine (3.0 mL, 37.5 mmol) in 15 min, the yellow mixture was stirred for 2 h at −42 °C. Ice was added to quench the reaction. The solution was acidified with aqueous 10% $NaHSO_4$. The aqueous layer was extracted with CH_2Cl_2 (3 × 20 mL). The organic fraction was washed with water, saturated $NaHCO_3$ and brine, dried over $MgSO_4$, filtered and evaporated under reduced pressure, and the residue was dissolved in 10 mL CH_3CN. $RuCl_3 \cdot xH_2O$ (10 mg), $NaIO_4$ (1.8 g, 8.3 mmol), H_2O (10 mL) were added to the solution at 0 °C. The solution was stirred for 15 min at 0 °C and returned to room temperature for 4 h. After the addition of Et_2O (10 mL) and brine (10 mL), the solution was extracted with Et_2O (3 × 20 mL). The organic fraction was washed with water, saturated $NaHCO_3$ and brine. The organic layer was dried over $MgSO_4$, filtered and evaporated under reduced pressure to yield L-Lan-**3**, D-Lan-**3**, L-MeLan-**3**, L-*allo*-MeLan-**3**, D-MeLan-**3**, and D-*allo*-MeLan-**3**.

Five mL TFA was added to the solution of L-Lan-**3**, D-Lan-**3**, L-MeLan-**3**, L-*allo*-MeLan-**3**, D-MeLan-**3**, and D-*allo*-MeLan-**3** in 5 mL CH_2Cl_2. After refluxing for 30 min, the volatiles were removed in vacuo to obtain L-Lan-**4**, D-Lan-**4**, L-MeLan-**4**, L-*allo*-MeLan-**4**, D-MeLan-**4**, and D-*allo*-MeLan-**4**.

L-Cysteine (0.7 g, 6 mmol) was added to the degassed solution of $KHCO_3$ (1.8 g, 18 mmol) in water (10 mL) followed by addition of L-Lan-**4**, D-Lan-**4**, L-MeLan-**4**, L-*allo*-MeLan-**4**, D-MeLan-**4**, and D-*allo*-MeLan-**4.** The solution was stirred for 16 h at rt. under nitrogen prior to addition of concentrated HCl

(10 mL, 100 mmol), and the resulted solution was heated under nitrogen at 70 °C for 5 h. The volatiles were removed in vacuo, and the resultant products were used without any further purification.

4.16. Advanced Marfey's analysis

Identification of amino acid residue chirality in peptides was performed using the methods described previously[31]. For lanthipeptides, 0.6 mg of each sample was hydrolyzed at 115 °C for 10 h in 600 μL of 6 mol/L HCl. The solution was lyophilized, which was redissolved in 500 μL water and lyophilized to remove HCl from the system. The hydrolysate was divided into two portions, which were incubated with 1 mol/L $NaHCO_3$ (150 μL) and 10 mg/mL L-FDLA (150 μL) at 37 °C for 90 min. After reaction, the solution was quenched with 2 mol/L HCl (150 μL) and diluted with MeCN (150 μL), and the resultant solutions were analyzed by LC−HRMS (Thermo Scientific, Acclaim™ 120 C18, 3 μm, 120 Å, 3 mm × 150 mm; 20%−100% CH_3CN in H_2O with 0.1% formic acid for 55 min; 0.3 mL/min).

Two portions of each commercial standard L-amino acid solution (50 μL, 50 mmol/L) were treated with 1 mol/L $NaHCO_3$ (20 μL) and 10 mg/mL L-FDLA (50 μL) at 37 °C for 90 min. After reaction, the solution was quenched with 2 mol/L HCl (10 μL) and diluted with MeCN (810 μL), which were analyzed by LC−HRMS using the same column and condition as above. The configuration of standard amino acids in lanthipeptides was determined by comparing the retention time of their DLA derivatives of with amino acid standards.

4.17. AlphaFold model of SslST and docking of **8**

The AlphaFold model of SslST was built using the online ColabFold server[39,40], and the resulted model was identical with the one from the UniProt database (UniProt identifier, AF-A0A2G1XES1-F1). Automated docking of **8** onto the SslST model were carried out using the Autodock Vina Chimera plugin[48,49]. Ligand coordinates were obtained using the "Build Structure" plugin of Chimera by inputting the SMILES string of **8**.

Acknowledgments

This work was supported by the National Natural Science Foundation of China (No. 21907047, 22077056, and 21907046), and the Fundamental Research Funds for the Central Universities (No. lzujbky2019-ct03, lzujbky-2019-10, and lzujbky-2021-ct05, China).

Author contributions

Meng Wang, Wen-Wei Li, Shangwen Luo, and Shi-Hui Dong designed experiments and wrote the manuscript with feedback from all authors; Zhe Cao synthesized the Lan and MeLan standards; Jianong Sun, Jiang Xiong, and Si-Qin Tao involved in the structural elucidation; Tinghong Lv performed anti-inflammatory and cytotoxicity assays; Kun Gao involved in discussion.

Conflicts of interest

The authors declare no conflicts of interest.

Appendix A. Supporting information

Supporting data to this article can be found online at https://doi.org/10.1016/j.apsb.2024.02.016.

References

1. Muttenthaler M, King GF, Adams DJ, Alewood PF. Trends in peptide drug discovery. *Nat Rev Drug Discov* 2021;**20**:309−25.
2. Tong Z, Xie X, Ge H, Jiao R, Wang T, Wang X, et al. Disulfide bridge-targeted metabolome mining unravels an antiparkinsonian peptide. *Acta Pharm Sin B* 2024;**14**:881−92.
3. Repka LM, Chekan JR, Nair SK, van der Donk WA. Mechanistic understanding of lanthipeptide biosynthetic enzymes. *Chem Rev* 2017;**117**:5457−520.
4. Arnison PG, Bibb MJ, Bierbaum G, Bowers AA, Bugni TS, Bulaj G, et al. Ribosomally synthesized and post-translationally modified peptide natural products: overview and recommendations for a universal nomenclature. *Nat Prod Rep* 2013;**30**:108−60.
5. Castiglione F, Lazzarini A, Carrano L, Corti E, Ciciliato I, Gastaldo L, et al. Determining the structure and mode of action of microbisporicin, a potent lantibiotic active against multiresistant pathogens. *Chem Biol* 2008;**15**:22−31.
6. Montalban-Lopez M, Scott TA, Ramesh S, Rahman IR, van Heel AJ, Viel JH, et al. New developments in RiPP discovery, enzymology and engineering. *Nat Prod Rep* 2021;**38**:130−239.
7. Rowe SM, Spring DR. The role of chemical synthesis in developing RiPP antibiotics. *Chem Soc Rev* 2021;**50**:4245−58.
8. Ongey EL, Yassi H, Pflugmacher S, Neubauer P. Pharmacological and pharmacokinetic properties of lanthipeptides undergoing clinical studies. *Biotechnol Lett* 2017;**39**:473−82.
9. van Staden ADP, van Zyl WF, Trindade M, Dicks LMT, Smith C. Therapeutic application of lantibiotics and other lanthipeptides: old and new findings. *Appl Environ Microbiol* 2021;**87**:e0018621.
10. Chapman E, Best MD, Hanson SR, Wong CH. Sulfotransferases: structure, mechanism, biological activity, inhibition, and synthetic utility. *Angew Chem Int Ed Engl* 2004;**43**:3526−48.
11. Guo Q, Xia H, Wu Y, Shao S, Xu C, Zhang T, et al. Structure, property, biogenesis, and activity of diterpenoid alkaloids containing a sulfonic acid group from *Aconitum carmichaelii*. *Acta Pharm Sin B* 2020;**10**:1954−65.
12. Luu DD, Joe A, Chen Y, Parys K, Bahar O, Pruitt R, et al. Biosynthesis and secretion of the microbial sulfated peptide RaxX and binding to the rice XA21 immune receptor. *Proc Natl Acad Sci U S A* 2019;**116**:8525−34.
13. Kenney GE, Rosenzweig AC. Genome mining for methanobactins. *BMC Biol* 2013;**11**:17.
14. El Ghazouani A, Basle A, Gray J, Graham DW, Firbank SJ, Dennison C. Variations in methanobactin structure influences copper utilization by methane-oxidizing bacteria. *Proc Natl Acad Sci U S A* 2012;**109**:8400−4.
15. Loughnan M, Bond T, Atkins A, Cuevas J, Adams DJ, Broxton NM, et al. alpha-conotoxin EpI, a novel sulfated peptide from Conus episcopatus that selectively targets neuronal nicotinic acetylcholine receptors. *J Biol Chem* 1998;**273**:15667−74.
16. Pruitt RN, Joe A, Zhang W, Feng W, Stewart V, Schwessinger B, et al. A microbially derived tyrosine-sulfated peptide mimics a plant peptide hormone. *New Phytol* 2017;**215**:725−36.
17. Pruitt RN, Schwessinger B, Joe A, Thomas N, Liu F, Albert M, et al. The rice immune receptor XA21 recognizes a tyrosine-sulfated protein from a Gram-negative bacterium. *Sci Adv* 2015;**1**:e1500245.
18. Kaas Q, Westermann JC, Craik DJ. Conopeptide characterization and classifications: an analysis using ConoServer. *Toxicon* 2010;**55**:1491−509.
19. Wu SJ, Chun MW, Shin KH, Toida T, Park Y, Linhardt RJ, et al. Chemical sulfonation and anticoagulant activity of acharan sulfate. *Thromb Res* 1998;**92**:273−81.

20. Men P, Geng C, Zhang X, Zhang W, Xie L, Feng D, et al. Biosynthesis mechanism, genome mining and artificial construction of echinocandin *O*-sulfonation. *Metab Eng* 2022;**74**:160−7.
21. Buhl AE, Waldon DJ, Baker CA, Johnson GA. Minoxidil sulfate is the active metabolite that stimulates hair follicles. *J Invest Dermatol* 1990; **95**:553−7.
22. Gerlt JA. Genomic enzymology: web tools for leveraging protein family sequence-function space and genome context to discover novel functions. *Biochemistry* 2017;**56**:4293−308.
23. Zallot R, Oberg N, Gerlt JA. Discovery of new enzymatic functions and metabolic pathways using genomic enzymology web tools. *Curr Opin Biotechnol* 2021;**69**:77−90.
24. Xue D, Older EA, Zhong Z, Shang Z, Chen N, Dittenhauser N, et al. Correlational networking guides the discovery of unclustered lanthipeptide protease-encoding genes. *Nat Commun* 2022;**13**:1647.
25. Acedo JZ, Bothwell IR, An L, Trouth A, Frazier C, van der Donk WA. *O*-Methyltransferase-mediated incorporation of a beta-amino acid in lanthipeptides. *J Am Chem Soc* 2019;**141**:16790−801.
26. Chen S, Xu B, Chen E, Wang J, Lu J, Donadio S, et al. Zn-dependent bifunctional proteases are responsible for leader peptide processing of class III lanthipeptides. *Proc Natl Acad Sci U S A* 2019;**116**:2533−8.
27. Blin K, Shaw S, Augustijn HE, Reitz ZL, Biermann F, Alanjary M, et al. antiSMASH 7.0: new and improved predictions for detection, regulation, chemical structures and visualisation. *Nucleic Acids Res* 2023;**51**:W46−50.
28. Blin K, Shaw S, Kloosterman AM, Charlop-Powers Z, van Wezel GP, Medema MH, et al. antiSMASH 6.0: improving cluster detection and comparison capabilities. *Nucleic Acids Res* 2021;**49**:W29−35.
29. Zhang SS, Xiong J, Cui JJ, Ma KL, Wu WL, Li Y, et al. Lanthipeptides from the same core sequence: characterization of a class II lanthipeptide synthetase from *Microcystis aeruginosa* NIES-88. *Org Lett* 2022;**24**:2226−31.
30. Huo L, van der Donk WA. Discovery and characterization of bicereucin, an unusual D-amino acid-containing mixed two-component lantibiotic. *J Am Chem Soc* 2016;**138**:5254−7.
31. Fujii K, Ikai Y, Oka H, Suzuki M, Ken-ichi H. A nonempirical method using LC/MS for determination of the absolute configuration of constituent amino acids in a peptide: combination of Marfey's method with mass spectrometry and its practical application. *Anal Chem* 1997; **69**:5146−51.
32. Harada K, Fujii K, Hayashi K, Suzuki M, Ikai Y, Oka H. Application of D,L-FDLA derivatization to determination of absolute configuration of constituent amino acids in peptide by advanced Marfey's method. *Tetrahedron Lett* 1996;**37**:3001−4.
33. Tan B, Zhang QB, Zhang LP, Zhu YG, Zhang CS. Functional characterization of the sulfotransferase TotS in totopotensamide biosynthesis. *Tetrahedron* 2022;**127**:133103−7.
34. Oliver RA, Li RF, Townsend CA. Monobactam formation in sulfazecin by a nonribosomal peptide synthetase thioesterase. *Nat Chem Biol* 2018;**14**:5−7.
35. Shi R, Lamb SS, Bhat S, Sulea T, Wright GD, Matte A, et al. Crystal structure of StaL, a glycopeptide antibiotic sulfotransferase from *Streptomyces toyocaensis*. *J Biol Chem* 2007;**282**:13073−86.
36. Gu LC, Wang B, Kulkarni A, Gehret JJ, Lloyd KR, Gerwick L, et al. Polyketide decarboxylative chain termination preceded by *O*-sulfonation in curacin A biosynthesis. *J Am Chem Soc* 2009;**131**:16033. +.
37. Tang X, Eitel K, Kaysser L, Kulik A, Grond S, Gust B. A two-step sulfation in antibiotic biosynthesis requires a type III polyketide synthase. *Nat Chem Biol* 2013;**9**:610−5.
38. Tanaka S, Nishiyori T, Kojo H, Otsubo R, Tsuruta M, Kurogi K, et al. Structural basis for the broad substrate specificity of the human tyrosylprotein sulfotransferase-1. *Sci Rep* 2017;**7**:8776.
39. Tunyasuvunakool K, Adler J, Wu Z, Green T, Zielinski M, Zidek A, et al. Highly accurate protein structure prediction for the human proteome. *Nature* 2021;**596**:590−6.
40. Mirdita M, Schutze K, Moriwaki Y, Heo L, Ovchinnikov S, Steinegger M. ColabFold: making protein folding accessible to all. *Nat Methods* 2022;**19**:679−82.
41. Holm L, Laiho A, Toronen P, Salgado M. DALI shines a light on remote homologs: one hundred discoveries. *Protein Sci* 2023;**32**: e4519.
42. Zhao S, Sakai A, Zhang X, Vetting MW, Kumar R, Hillerich B, et al. Prediction and characterization of enzymatic activities guided by sequence similarity and genome neighborhood networks. *Elife* 2014;**3**: e03275.
43. Zallot R, Oberg N, Gerlt JA. The EFI web resource for genomic enzymology tools: leveraging protein, genome, and metagenome databases to discover novel enzymes and metabolic pathways. *Biochemistry* 2019;**58**:4169−82.
44. Shannon P, Markiel A, Ozier O, Baliga NS, Wang JT, Ramage D, et al. Cytoscape: a software environment for integrated models of biomolecular interaction networks. *Genome Res* 2003;**13**:2498−504.
45. Claesen J, Bibb M. Genome mining and genetic analysis of cypemycin biosynthesis reveal an unusual class of posttranslationally modified peptides. *Proc Natl Acad Sci U S A* 2010;**107**:16297−302.
46. Surh YJ, Chun KS, Cha HH, Han SS, Keum YS, Park KK, et al. Molecular mechanisms underlying chemopreventive activities of anti-inflammatory phytochemicals: down-regulation of COX-2 and iNOS through suppression of NF-kappa B activation. *Mutat Res* 2001; **480**−**481**:243−68.
47. Denoel T, Zervosen A, Gerards T, Lemaire C, Joris B, Blanot D, et al. Stereoselective synthesis of lanthionine derivatives in aqueous solution and their incorporation into the peptidoglycan of *Escherichia coli*. *Bioorg Med Chem* 2014;**22**:4621−8.
48. Trott O, Olson AJ. AutoDock Vina: improving the speed and accuracy of docking with a new scoring function, efficient optimization, and multithreading. *J Comput Chem* 2010;**31**:455−61.
49. Pettersen EF, Goddard TD, Huang CC, Couch GS, Greenblatt DM, Meng EC, et al. UCSF Chimera−a visualization system for exploratory research and analysis. *J Comput Chem* 2004;**25**:1605−12.